frontiers | Frontiers in Materials

TYPE Original Research
PUBLISHED 02 September 2022
DOI 10.3389/fmats.2022.966535

OPEN ACCESS

EDITED BY
Huifang Zhang,
University of Cambridge,
United Kingdom

REVIEWED BY
Yongzhi Cheng,
Wuhan University of Science and Technology, China
Tingting Liu,
University of Shanghai for Science and Technology, China
Weiren Zhu,
Shanghai Jiao Tong University, China

*CORRESPONDENCE
Quan Li,
quanli@tute.edu.cn
Shuang Wang,
wangshuang@tute.edu.cn

SPECIALTY SECTION
This article was submitted to Metamaterials, a section of the journal Frontiers in Materials

RECEIVED 11 June 2022
ACCEPTED 01 August 2022
PUBLISHED 02 September 2022

CITATION
Li Q, Su H, Zhu J and Wang S (2022), Active control of dual electromagnetically induced transparency in terahertz graphene-metal hybrid metasurfaces. *Front. Mater.* 9:966535. doi: 10.3389/fmats.2022.966535

Active control of dual electromagnetically induced transparency in terahertz graphene-metal hybrid metasurfaces

Quan Li[1]*, Hao Su[1], Jun Zhu[2] and Shuang Wang[1]*

[1]School of Electronic Engineering, Tianjin University of Technology and Education, Tianjin, China, [2]School of Optical and Electronical Information, Zhongshan Torch Polytechnic, Zhongshan, China

Active control of electromagnetically induced transparency (EIT) using metasurfaces has attracted growing interests in recent years, especially the ones that have multiple EIT windows. Here, we give out a metallic metasurface design that can achieve dual EIT (D-EIT) in the terahertz (THz) regime, and propose a strategy to individually and simultaneously control the two windows by integrating graphene structures into the design. The near-field simulations indicate that the physical mechanism lies in the composite effect of conductive graphene. The theoretical analysis reveals that the active modulation is attributed to the changes in the damping rates of the dark modes and the coupling coefficients between bright mode and dark modes. The proposed graphene-metal hybrid metasurfaces provide a way for designing compact dual-band slow-light and modulation devices, which may find potential applications in dual-frequency-channel THz wireless communications.

KEYWORDS

electromagnetically induced transparency, dual windows, metasurface, graphene-metal hybrid, active, terahertz

Introduction

Metasurfaces are two-dimensional version of metamaterials, which are composed of planar subwavelength artificial structures at the interface. They have ultra-high degree of freedom in designing the propagations of electromagnetic waves, and have attracted enormous research interest over the whole electromagnetic field (Glybovski et al., 2016; Sun et al., 2019). The internal working mechanism of metasurfaces is to use the local resonance-determined phase, amplitude and polarization manipulation ability of the composed meta-atoms to control the spectral responses and wavefronts of the output waves (Wang et al., 2015; Meng et al., 2019; Han and Chen, 2020; Sun et al., 2020; Venkatesh et al., 2020; He et al., 2021; Kim et al., 2021). Among them, one potential application of metasurfaces is to mimic the quantum phenomena as it offers a smart route to achieve corresponding optical modulations in a classical way.

Recently, analogues of quantum phenomenon of electromagnetically induced transparency (EIT) behavior using metasurfaces have attracted enormous attention (Gu et al., 2012; Xiao et al., 2018; Li et al., 2020). Various artificial structures have been adopted, such as bar structures, multi-layer fish scale structures, cut wire plus split ring resonator (SRR) combinations, and Fano resonators, etc. The typical way to realize these analogues is to construct coupled bright and dark resonators. A reasonable combination of them can realize destructive interference in the bright mode and thus form an EIT window. However, the combination of one bright mode and one dark mode can only generate a single EIT window. To meet more complex application requirements, it is eager to achieve the EIT effect with multiple transparency windows and endow it with tunable features at the same time (Liu et al., 2018a; Gao et al., 2019; Liu et al., 2021; Jiang et al., 2022; Zhuo et al., 2022).

Graphene, composed of single-layer carbon atom structures, has emerged as an attractive functional two-dimensional material. It has been widely applied to integrate with metasurfaces and tune their responses, as its conductivity is directly determined by its Fermi energy which can be freely controlled through chemical, optical, and electrical doping methods. So far, various graphene-based active metasurfaces have been successfully demonstrated, such as modulators (Li et al., 2015; Zhang et al., 2022a), absorbers (Chen et al., 2020; Cheng et al., 2020), lenses (Wang et al., 2021a; Zhu et al., 2022a; Zhu et al., 2022b), polarization controllers (Cheng et al., 2021; Zhang et al., 2022b), as well as EIT analogues we focus here (Kim et al., 2018; Xiao et al., 2020; Zhang et al., 2021). Among the reported active EIT metasurfaces, there are only a few works on the control of dual EIT (D-EIT) windows using graphene (Ge et al., 2020; Zhang et al., 2020; Mei et al., 2021). They can be roughly divided into three categories: 1) Apply graphene to compose the structure (Liu et al., 2019a; Liu et al., 2019b; Gao et al., 2019), which requires very high-quality graphene that can hardly be achieved in real cases. 2) Hybrid a whole monolayer graphene onto metallic structures (Liu et al., 2018b), which can ensure the modulation of resonance but will bring additional background transmission loss in the off-resonance range (Li et al., 2015). 3) Pattern graphene into structures and integrate them at particular places of the metal structures (Wu et al., 2021a), which can overcome the above limitations simultaneously.

In this work, we theoretically propose an active D-EIT device using hybrid graphene-metal metasurfaces in the terahertz regime. The unit cell of the metal part consists of a bright mode resonator composed of a cut-wire resonator (CWR), and two dark mode resonators composed of a double-split ring resonator (DSRR) and a double-U resonator (DUR), respectively. Such a design allows generation of D-EIT windows. By integrating graphene structures separately and simultaneously into the two dark mode resonators, active and selective modulations of the two EIT windows are achieved.

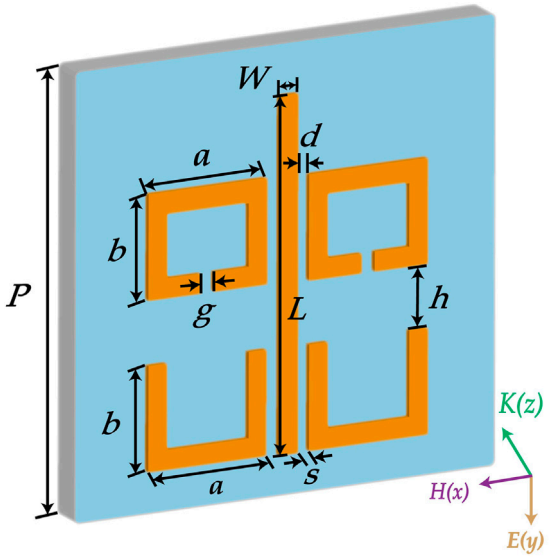

FIGURE 1
The unit cell of the proposed D-EIT metasurface with incident plane wave.

Near-field simulations and theoretical fittings reveal that such modulations are caused by the shorting effects of the graphene structures to the capacitive gaps of the dark mode resonators, which modify their resonance damping rates and coupling coefficients to the bright mode resonator. Our approach could have potential applications in designing a variety of future photonic devices.

Design of the dual electromagnetically induced transparency metasurface

The unit cell of the designed D-EIT metasurface is schematically illustrated in Figure 1. A metal structure that consists of a CWR, a DSRR, and a DUR made from 200 nm-thick aluminum is placed on a 550 μm-thick silicon substrate. The two split ring resonators (SRRs) in the DSRR and the two U-shaped resonators in the DUR are symmetrically placed on the left and right sides of the CWR with distances of d and s, respectively. The corresponding specific geometric parameters are: L = 65 μm,W = 5 μm, a = 25 μm, b = 23 μm, g = 1 μm, h = 8.5 μm, d = 1 μm, s = 1 μm, and P = 100 μm. To characterize its transmission response, numerical simulations based on finite-element time-domain (FDTD) method are carried out, in which the aluminum is set with a constant conductivity of $\sigma = 3.56 \times 10^7$ S/m, the substrate is modeled as a lossless dielectric with $\varepsilon = 11.9$, the boundary conditions are periodic along x and y directions while open along z directions, and a plane wave is set as the terahertz source

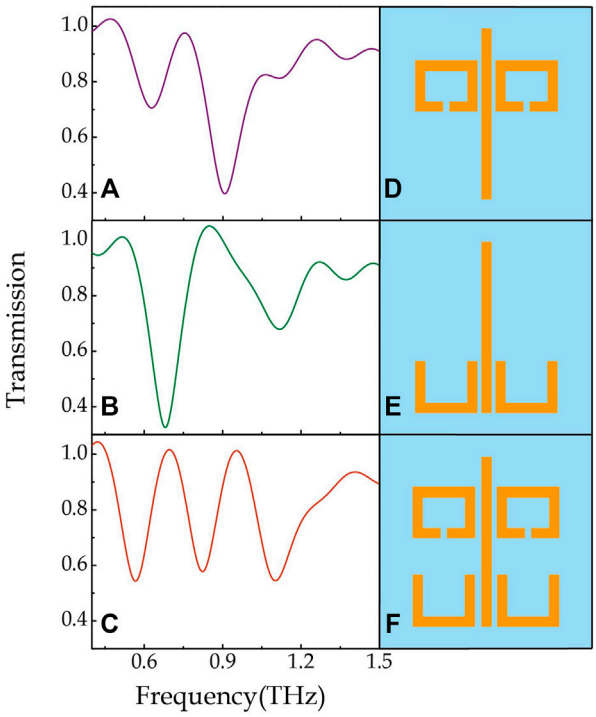

FIGURE 2
Simulated amplitude transmission spectra of **(A)** "CWR + DSRR", **(B)** "CWR + DUR", and **(C)** D-EIT metasurfaces under the *y*-polarized incidences. **(D–F)** Schematics of the unit cells corresponding to **(A–C)**, respectively.

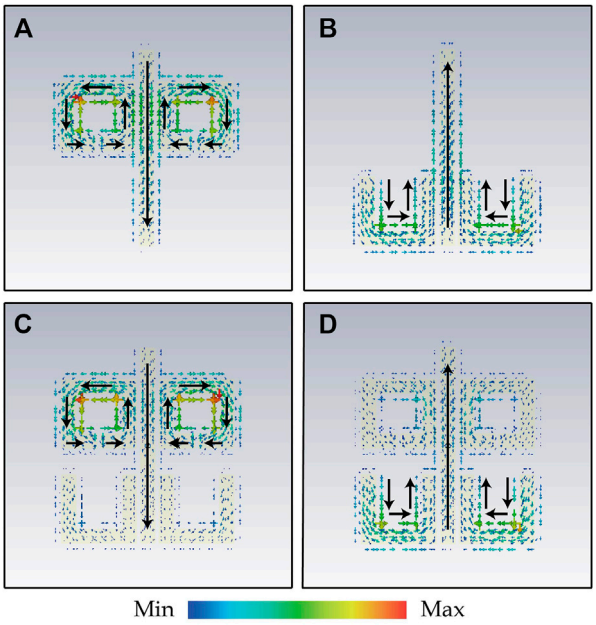

FIGURE 3
Surface current distributions of the **(A)** "CWR + DSRR" at the transparency peak of 0.753 THz, **(B)** "CWR + DUR" at the transparency peak of 0.849 THz, **(C)** D-EIT at the transparency peak 1 at 0.696 THz, **(D)** D-EIT at the transparency peak 2 at 0.954 THz, under the *y*-polarized incidences.

which normally illuminates onto the metasurface along the $+z$ direction.

Under *y*-polarized incidence, the CWR can be strongly excited and functions as the bright mode, whereas the DSRR and DUR cannot and thus function as the dark modes (Gu et al., 2012; Liu et al., 2012; Xiao et al., 2018; Li et al., 2020; Shu and Mei, 2022). Their coupling effects would give birth to EIT effects, as indicated by the transmission spectra in Figure 2. When there are only the CWR and DSRR (CWR + DSRR, see Figure 2D), a single EIT peak at 0.753 THz is emerged, as shown in Figure 2A. When there are only the CWR and DUR (CWR + DUR, see Figure 2E), a similar phenomenon happens but the EIT peak appears at a higher frequency of 0.849 THz (see Figure 2B). The most interesting thing happens when the three resonators all exist (CWR + DSRR + DUR, see Figure 2F), D-EIT effect occurs with two EIT peaks respectively appearing at 0.696 THz (peak 1) and 0.954 THz (peak 2).

Further evidences of the above EIT effects can be seen in the simulated surface current distributions at the corresponding EIT peak frequencies in Figure 3, where the resonances of the bright mode resonator are all strongly suppressed by the near-field coupling effects whereas the resonances of the dark mode resonator become dominate. Specifically, they show that the two EIT peaks at the lower and higher frequencies in the D-EIT case are separately caused by the couplings from the DSRR and DUR. The whole physical process can be expressed as follows: under *y*-polarized incidence, the electric dipole resonance of the CWR is directly excited; it then generates electric coupling fields at its two ends while magnetic coupling fields at its center, these coupling fields could excite the magnetic dipole resonances of the DSRR and DUR when they are placed around the CWR; after that, the resonance fields of the DSRR and DUR couple back to the CWR and suppress its resonance due to the interference cancellation effect; finally, at the frequencies that the cancellations happen, EIT windows occur. It should be noted that the magnetic resonance frequencies of the DSRR and DUR are different here, so their corresponding EIT windows locate at different frequencies, forming the D-EIT effect.

Passive control of the electromagnetically induced transparency peaks

For the purpose of showing the modulation ability of the D-EIT, three sets of unit cells are proposed and characterized

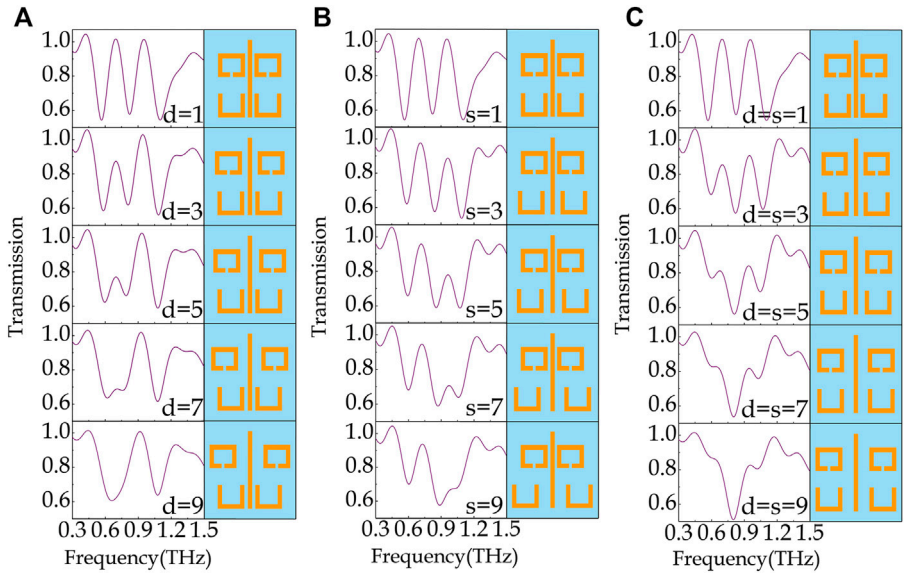

FIGURE 4
Simulated amplitude transmission spectra (left column) and schematics of the unit cells (right column) with **(A)** d varied from 1 to 9 μm with an interval of 2 μm and s fixed at 1 μm, **(B)** s varied from 1 to 9 μm with an interval of 2 μm and d fixed at 1 μm, **(C)** d and s simultaneously varied from 1 to 9 μm with an interval of 2 μm.

by changing d or (and) s, as illustrated in Figure 4. As d gradually increases from 1 to 9 μm, see the right column of Figure 4A, the two SRRs in the DSRR get away from the CWR, resulting in reduced coupling strength between the DSRR and the CWR. Therefore, the amplitude of peak 1 gradually shrinks until completely disappears, see the left column of Figure 4A. Specifically, the amplitude of peak 1 changes from 1 to 0.61, corresponding to a modulation depth of $\Delta T_1 = 39\%$. Here the modulation depth is defined as $\Delta T_i = |(T_0 - T_g)/T_0| \times 100\%$ with T_0 and T_g being the maximum and minimum values of the amplitude of the EIT peak, and the subscript i representing peak i ($i = 1, 2$). Since the coupling between the DUR and the CWR remains, the amplitude of peak 2 keeps unchanged. A similar phenomenon can also be observed for the case of gradually increasing s from 1 to 9 μm, where the amplitude of peak 2 undergoes a significant decrease from 1 to 0.67 with a modulation depth of $\Delta T_2 = 33\%$, while that of peak 1 nearly unchanged, see Figure 4B. Such modulation behaviors indicate that peak 1 and peak 2 can be separately modulated. Meanwhile, this also indicates that the two peaks can be simultaneously modulated by changing d and s at the same time. As illustrated in Figure 4C, the amplitudes of both peaks decrease as d and s simultaneously increase from 1 to 9 μm. The corresponding amplitudes change from 1 to 0.86 (peak 1) and 1 to 0.83 (peak 2), whereas the modulation depths are $\Delta T_1 = 14\%$ and $\Delta T_2 = 17\%$, respectively.

Active control of the electromagnetically induced transparency peaks

To achieve active control of the transmission peaks, another three sets of unit cells are further designed by integrating monolayer graphene structures into the gaps of the DSRR, the DUR, and between the DSRR and the DUR, see Figures 5A–C. We denote them as D-EIT-g1, D-EIT-g2 and D-EIT-g12, respectively. To simulate their responses, the Kubo formula is used to model the complex optical conductivity of graphene $\sigma(\omega) = \sigma_{\text{intra}}(\omega) + \sigma_{\text{inter}}(\omega)$ (Chen and Alù, 2011; Zhang et al., 2015):

$$\sigma_{\text{intra}}(\omega) = i\frac{e^2 K_B T}{\pi\hbar^2(\omega + i\tau^{-1})}\left[\frac{E_F}{K_B T} + 2\ln\left(\exp\left(-\frac{E_F}{K_B T}\right) + 1\right)\right], \quad (1)$$

$$\sigma_{\text{inter}}(\omega) = i\frac{e^2}{4\pi\hbar}\ln\left[\frac{2|E_F| - \hbar(\omega + i\tau^{-1})}{2|E_F| + \hbar(\omega + i\tau^{-1})}\right]. \quad (2)$$

where $\sigma_{\text{intra}}(\omega)$ and $\sigma_{\text{inter}}(\omega)$ respectively represent the contributions from the intraband electron-photon scattering and the direct interband electron transition, e is the electron charge, K_B is the Boltzmann constant, T is the temperature, $\hbar$ is the reduced Planck's constant, E_F is the Fermi energy, τ is the momentum relaxation time. In the terahertz band, owing to the small photon energy, the conductivity of graphene is dominated

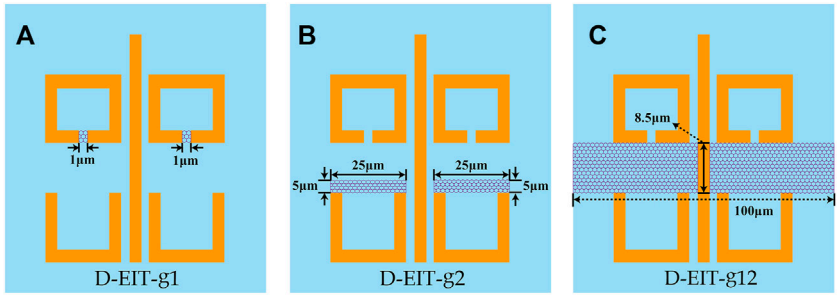

FIGURE 5
Schematics of the unit cells of **(A)** D-EIT-g1, **(B)** D-EIT-g2, **(C)** D-EIT-g12.

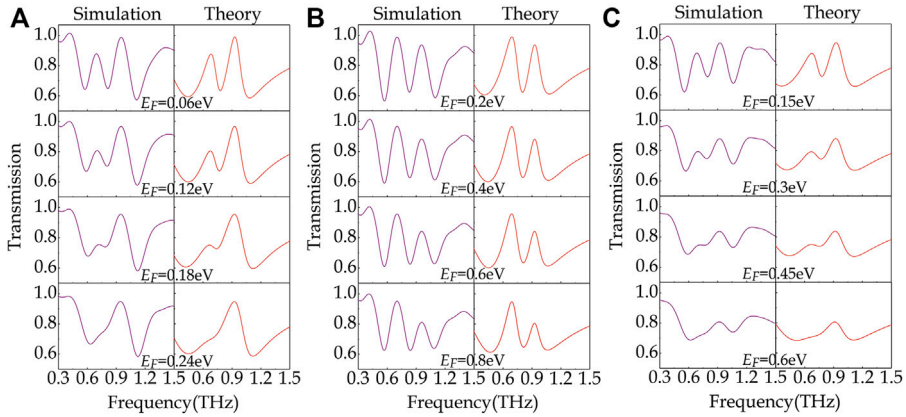

FIGURE 6
Simulated (left column) and calculated (right column) amplitude transmission spectra of **(A)** D-EIT-g1, **(B)** D-EIT-g2, **(C)** D-EIT-g12 at various E_F.

by the intraband process, i.e., $\sigma(\omega) = \sigma_{intra}(\omega)$ (Chen and Alù, 2011; Cheng et al., 2020). When τ is fixed, the conductivity would increase as E_F increases (Chen and Alù, 2011; Zhang et al., 2015; Wang et al., 2021a). Here, we set τ as a constant of 25 fs to be consistent with the range of measured results (Lee et al., 2012; Liu et al., 2015; Li et al., 2019). In simulation, graphene is modeled as a two-dimensional conductive sheet with zero thickness (Liu et al., 2019b; Wang et al., 2021b), since the thickness becomes not essential as long as it is extremely small compared to the wavelength of interest (Vakil and Engheta, 2011).

The left columns in Figure 6 illustrate the corresponding simulated amplitude transmission spectra. It can be seen that the EIT peaks can be actively modulated as E_F gradually changes. In the case of D-EIT-g1, the amplitude of peak 1 can be switched from 0.88 to 0.67 as E_F slightly increases from 0.06 to 0.24 eV, corresponding to a modulation depth of $\Delta T_1 = 24\%$, whereas that of peak 2 almost unchanged, see the left column of Figure 6A. In the case of D-EIT-g2, it is found that the amplitude of peak 1 only changes a little, while that of peak 2 undergoes an obvious modulation from 0.94 to 0.81 as E_F increases from 0.2 to 0.8 eV, corresponding to a modulation depth of $\Delta T_2 = 14\%$, see left column of Figure 6B. In the case of D-EIT-g12, the response combines those of the former two cases, where the amplitudes of both peaks decrease as E_F increases from 0.15 to 0.6 eV, see left column of Figure 6C. In particular, when E_F reaches 0.6 eV, peak 1 disappears while peak 2 leaves a small hill. Specifically, the amplitude of peak 1 (2) reduces from 0.88 (0.95) to 0.69 (0.81), corresponding to a modulation depth of $\Delta T_1 = 22\%$ ($\Delta T_2 = 15\%$). Although these modulation depths are not as high as those of previous works (Wu et al., 2021a), we here can realize the on-to-off EIT peak modulation with a lower E_F, for example, 0.24 eV. The above results also indicate that the gap in the DSRR is more sensitive to the graphene conductivity than that in DUR.

To understand the above modulation behavior, a qualitative analysis based on simulated surface current distributions at the EIT peaks is proposed, as shown in Figure 7. It is clearly seen that as E_F

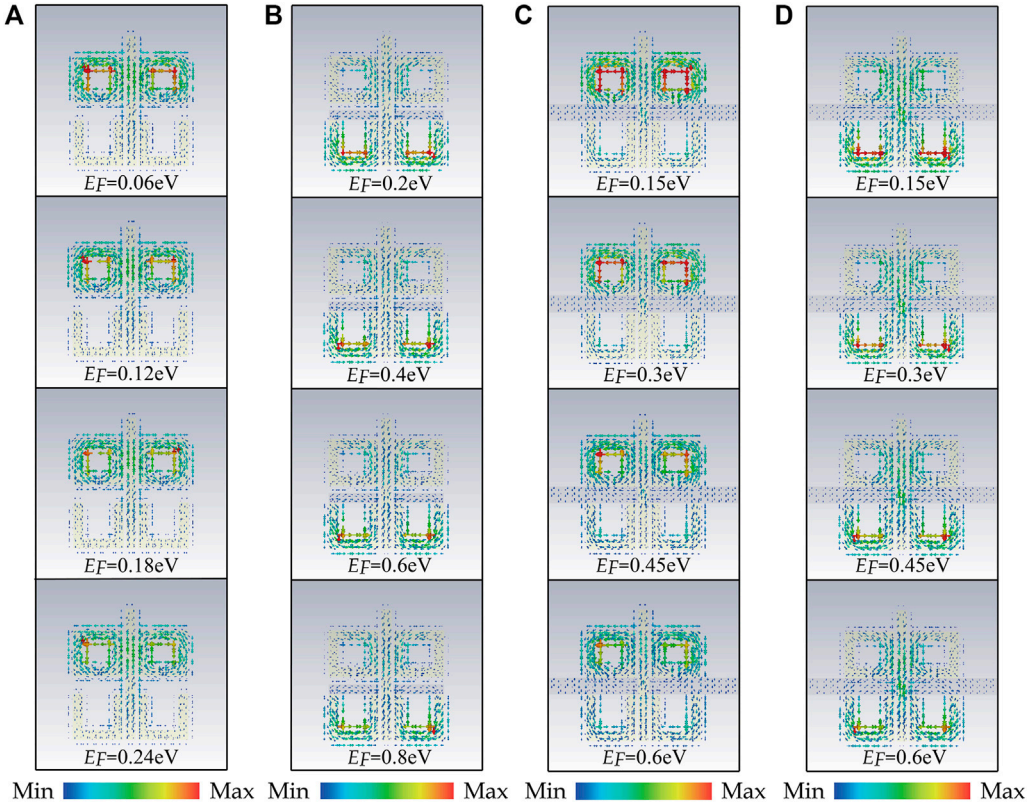

FIGURE 7
Surface current distributions of **(A)** D-EIT-g1 at the peak 1 frequency with E_F varied from 0.06 to 0.24 eV, **(B)** D-EIT-g2 at the peak 2 frequency with E_F varied from 0.2 to 0.8 eV, **(C)** D-EIT-g12 at the peak 1 frequency with E_F varied from 0.15 to 0.6 eV, **(D)** D-EIT-g12 at the peak 2 frequency with E_F varied from 0.15 to 0.6 eV.

increases, the surface currents on the DSRR or (and) DUR decrease. The circulating surface currents in the DSRR and DUR imply large carrier aggregation at the gaps. Therefore, the graphene in the gaps can short their surface currents. The larger E_F is, the larger the graphene conductivity becomes, and the stronger shorting effect occurs. Thus, as E_F increases, the coupling excited resonances become weaker, leading to reduced suppressed fields to the CWR. Therefore, the amplitudes of the EIT peaks decrease. Since the gaps in the DSRR structure are smaller than that of DUR, the surface currents can be more easily shorted, thus the amplitude modulation on peak 1 is stronger, whereas the amplitude modulation on peak 2 is mild due to the wider gap in DUR.

In order to further elucidate the inner physical mechanism of the above active modulation behaviors, a coupled oscillator model is applied to quantitatively describe the near field coupling between the CWR and the DSRR and the DUR (Su et al., 2015; Jiang et al., 2022):

$$\begin{aligned} &\ddot{x}_1 + \gamma_1\dot{x}_1 + \omega_1^2 x_1 + \kappa_{12}x_2 + \kappa_{13}x_3 = gE, \\ &\ddot{x}_2 + \gamma_2\dot{x}_2 + \omega_2^2 x_2 + \kappa_{12}x_1 + \kappa_{23}x_3 = 0, \\ &\ddot{x}_3 + \gamma_3\dot{x}_3 + \omega_3^2 x_3 + \kappa_{23}x_2 + \kappa_{13}x_1 = 0, \end{aligned} \tag{3}$$

where x_1, x_2, x_3, γ_1, γ_2, γ_3, ω_1, ω_2 and ω_3 represent the resonance amplitudes, the damping rates, and the resonance frequencies of the resonance modes of CWR, DSRR and DUR, respectively; κ_{12}, κ_{13} and κ_{23} represent the coupling coefficients between the resonances of CWR and DSRR, CWR and DUR, DSRR and DUR, respectively; g is the geometric parameter describing the coupling strength of the CWR with the incident field E. By solving Eq. 3, x_1, x_2 and x_3 can be obtained. Then, the transmission can be calculated by:

$$\tilde{t}(\omega) = \frac{c(1+n_{sub})}{c(1+n_{sub}) - i\omega\chi_e}, \tag{4}$$

where c is the light velocity in vacuum, n_{sub} is the refractive index of the substrate, χ_e is the susceptibility of the D-EIT structure which is proportional to the bright mode x_1 (Zhang et al., 2008; Gu et al., 2012; Su et al., 2015). The corresponding fitting results are illustrated in the right columns of Figure 6, whose varying features are in good agreement with the simulated results. The discrepancies between the simulation and theoretical results can be attributed to the complex interaction process in the

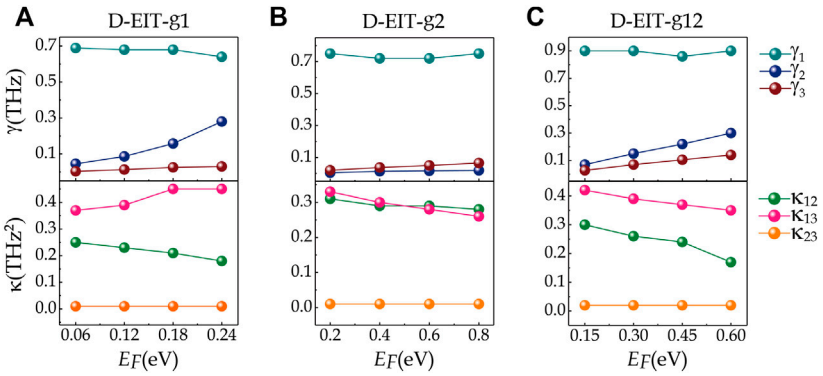

FIGURE 8
Theoretical fitting values of the electromagnetic parameters γ_1, γ_2, γ_3, κ_{12}, κ_{13}, and κ_{23} under different E_F for **(A)** D-EIT-g1, **(B)** D-EIT-g2, **(C)** D-EIT-g12.

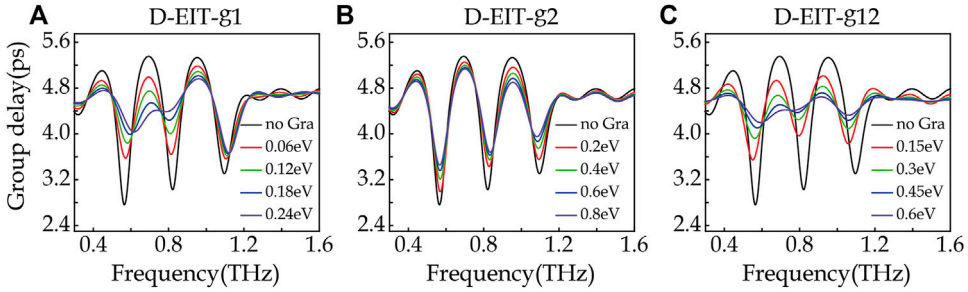

FIGURE 9
Group delay spectra as a function of E_F for **(A)** D-EIT-g1, **(B)** D-EIT-g2, **(C)** D-EIT-g12.

proposed coupling system, where our coupling model of Eq. 3 cannot fully describe the interaction details (Gao et al., 2022). The fitting parameters with respect to E_F are plotted in Figure 8. It is observed that the values of γ_1 are much higher than those of γ_2 and γ_3 for all cases, which change mildly since the graphene structures have little effect on the resonances of the CWR, whereas γ_2 increases obviously in D-EIT-g1, γ_3 gently rises in D-EIT-g2, and both γ_2 and γ_3 undergo a rise in D-EIT-g12 as E_F increases. The above variation trends in γ_2 and γ_3 verify that the DSRRs are more sensitive to the graphene conductivity and thus peak 1 has a larger modulation depth. These behaviors verify the above-mentioned shorting effects of the graphene structures on the gaps of the DSRR and DUR. As for the coupling coefficients, κ_{12} decreases and κ_{13} increases in D-EIT-g1, while both κ_{12} and κ_{13} decrease in D-EIT-g2 and D-EIT-g12. Thus, it can be obtained that the active modulation of the EIT peaks is arisen from the changes in the damping rates of the dark modes (DSRR and DUR) and coupling coefficients between the bright mode and dark modes.

Next, the modulation effects on the slow-light behavior of our designs are investigated by calculating the corresponding group delay τ_g as (Li et al., 2020; Wu et al., 2021a):

$$\tau_g = \frac{d\varphi}{d\omega} - \frac{d\varphi_0}{d\omega}, \tag{5}$$

where $d\varphi/d\omega$ and the $d\varphi_0/d\omega$ are the group delays of the D-EIT metasurface and the vacuum with the same thickness, respectively. Figure 9 shows that the group delays of peak 1 and peak 2 achieve 5.4 and 5.3 ps with the absence of graphene, which is comparable with the previous D-EIT works (Wu et al., 2021a; Wu et al., 2021b; Mei et al., 2021). When graphene is integrated into the unit cell of structure, active modulation of the group delay is observed. In D-EIT-g1, the group delay at peak 1 decreases dramatically from 5.4 to 4.4 ps as E_F increases from 0.06 to 0.24 eV, while that at peak 2 reduces slightly, as shown in Figure 9A. In D-EIT-g2, the group delay at peak 2 gradually decreases from 5.3 to 4.9 ps as E_F increases from 0.2 to 0.8 eV, while that at peak 1 decreases slightly, as shown in

Figure 9B. In D-EIT-g12, the group delays at both peaks decrease dramatically from 5.4 to 4.4 ps (peak 1) and from 5.3 to 4.6 ps (peak 2) as E_F increases from 0.15 to 0.6 eV, as shown in Figure 9C. Consequently, active modulation of slow-light effects in D-EIT windows can be accomplished using our method.

Discussion

Although the above design and analysis are mainly carried out in theory, the potential experiments are possibly carried out (Wang et al., 2019). For the sample fabrication, the aluminum structures could be fabricated onto a silicon substrate using traditional photolithography and metal evaporation methods, while the graphene structures could be obtained by firstly transferring a large-area chemical vapor deposition (CVD) graphene onto the structures and then shaping into desired patterns using photolithography and oxygen plasma etching methods. For the sample characterization, a terahertz time-domain spectroscopy system could be applied to measure the transmission spectra. In order to tune the conductivity of graphene, optical pump or chemical doping could be applied (Novoselov et al., 2012; Weis et al., 2012). If electric doping is adopted, the graphene patches can be extended to graphene ribbons along the direction perpendicular to the CWR to allow external voltage bias, where our further simulations show the transmission features almost remain (not presented) as it nearly does not interact with the incident field as compared to most of the previous D-EIT works (Zhang et al., 2020; Wu et al., 2021a).

Conclusion

In conclusion, we theoretically demonstrated a D-EIT metasurface design which can simultaneously generate two EIT windows by engineering the couplings between one bright mode and two dark modes in the terahertz regime. By controlling the relative distances between the bright and dark modes, the two EIT peaks can be individually and simultaneously switched in a passive way. More important, by integrating graphene structures into the gaps of the dark modes to form metal-graphene hybrid metasurfaces, the two EIT peaks can also be individually and simultaneously modulated in an active way by tuning E_F of the graphene. A coupled oscillator model is also proposed which can well describe the simulated transmission responses. The group delays reach 5.4 and 5.3 ps at the two EIT peaks, which is comparable with those in previous D-EIT works. Thanks to the advantages of the structure where the dark mode resonators are symmetrically placed at the two sides of the CWR, electrical control is possible by extending the graphene patches to graphene ribbons along the direction perpendicular to the CWR which can help avoid extra resonance loss. Our method provides an effective way to generate and modulate D-EIT peaks for various related applications.

Data availability statement

The raw data supporting the conclusions of this article will be made available by the authors, without undue reservation.

Author contributions

QL and HS conceived the original idea. QL, HS, and JZ completed numerical simulations. QL, HS, JZ, and SW analyzed the simulated and fitted results. QL and SW supervised the theory. All the authors discussed the results and contributed to the writing of the manuscript.

Funding

This work was supported by the National Natural Science Foundation of China (61705167), the project for the young innovative talents in colleges and universities of Guangdong (2019GKQNCX136), the Scientific Research Project of Tianjin Municipal Education Commission (2020KJ125).

Acknowledgments

We also thank for the support from Tianjin Key Laboratory of Imaging and Sensing Microelectronic Technology.

Conflict of interest

The authors declare that the research was conducted in the absence of any commercial or financial relationships that could be construed as a potential conflict of interest.

Publisher's note

References

Chen, F., Cheng, Y., and Luo, H. (2020). A broadband tunable terahertz metamaterial absorber based on single-layer complementary gammadion-shaped graphene. *Materials* 13, 860. doi:10.3390/ma13040860

Chen, P.-Y., and Alù, A. (2011). Atomically thin surface cloak using graphene monolayers. *ACS Nano* 5 (7), 5855–5863. doi:10.1021/nn201622e

Cheng, Y., Zhao, H., and Li, C. (2020). Broadband tunable terahertz metasurface absorber based on complementary-wheel-shaped graphene. *Opt. Mat. (Amst).* 109, 110369. doi:10.1016/j.optmat.2020.110369

Cheng, Y., Zhu, X., Li, J., Chen, F., Luo, H., and Wu, L. (2021). Terahertz broadband tunable reflective cross-polarization convertor based on complementary cross-shaped graphene metasurface. *Phys. E Low-dimensional Syst. Nanostructures* 134, 114893. doi:10.1016/j.physe.2021.114893

Gao, C., Sun, Y., and Zhang, H. (2022). Tunable dual-band linear-to-circular polarization conversion based on the electromagnetically induced transparency utilizing the graphene metamaterial. *Phys. E Low-dimensional Syst. Nanostructures* 141, 115225. doi:10.1016/j.physe.2022.115225

Gao, E., Liu, Z., Li, H., Xu, H., Zhang, Z., Luo, X., et al. (2019). Dynamically tunable dual plasmon-induced transparency and absorption based on a single-layer patterned graphene metamaterial. *Opt. Express* 27, 13884–13894. doi:10.1364/OE.27.013884

Ge, J., You, C., Feng, H., Li, X., Wang, M., Dong, L., et al. (2020). Tunable dual plasmon-induced transparency based on a monolayer graphene metamaterial and its terahertz sensing performance. *Opt. Express* 28, 31781–31795. doi:10.1364/OE.405348

Glybovski, S. B., Tretyakov, S. A., Belov, P. A., Kivshar, Y. S., and Simovski, C. R. (2016). Metasurfaces: From microwaves to visible. *Phys. Rep.* 634, 1–72. doi:10.1016/j.physrep.2016.04.004

Gu, J., Singh, R., Liu, X., Zhang, X., Ma, Y., Zhang, S., et al. (2012). Active control of electromagnetically induced transparency analogue in terahertz metamaterials. *Nat. Commun.* 3, 1151. doi:10.1038/ncomms2153

Han, J., and Chen, R. (2020). Tunable broadband terahertz absorber based on a single-layer graphene metasurface. *Opt. Express* 28, 30289–30298. doi:10.1364/OE.403631

He, Z., Li, L., Ma, H., Pu, L., Xu, H., Yi, Z., et al. (2021). Graphene-based metasurface sensing applications in terahertz band. *Results Phys.* 21, 103795. doi:10.1016/j.rinp.2020.103795

Jiang, N., Zhang, Z., Liang, W., Deng, Y., Zhang, P., Zhang, C., et al. (2022). Analysis of evolution of coupled Lorentz resonances and their sensing properties in terahertz metamaterials. *Front. Phys.* 10, 840090. doi:10.3389/fphy.2022.840090

Kim, M., Kim, S., and Kim, S. (2021). Ultra-compact integrated terahertz modulator based on a graphene metasurface. *Opt. Lett.* 46, 605–608. doi:10.1364/OL.401969

Kim, T. T., Kim, H. D., Zhao, R., Oh, S. S., Ha, T., Chung, D. S., et al. (2018). Electrically tunable slow light using graphene metamaterials. *ACS Photonics* 5 (5), 1800–1807. doi:10.1021/acsphotonics.7b01551

Lee, S. H., Choi, M., Kim, T.-T., Lee, S., Liu, M., Yin, X., et al. (2012). Switching terahertz waves with gate-controlled active graphene metamaterials. *Nat. Mat.* 11, 936–941. doi:10.1038/nmat3433

Li, Q., Tian, Z., Zhang, X., Xu, N., Singh, R., Gu, J., et al. (2015). Dual control of active graphene-silicon hybrid metamaterial devices. *Carbon* 90, 146–153. doi:10.1016/j.carbon.2015.04.015

Li, S., Nugraha, P. S., Su, X., Chen, X., Yang, Q., Unferdorben, M., et al. (2019). Terahertz electric field modulated mode coupling in graphene-metal hybrid metamaterials. *Opt. Express* 27, 2317–2326. doi:10.1364/OE.27.002317

Li, Q., Liu, S., Zhang, X., Wang, S., and Chen, T. (2020). Electromagnetically induced transparency in terahertz metasurface composed of meanderline and U-shaped resonators. *Opt. Express* 28, 8792–8801. doi:10.1364/OE.389292

Liu, X., Gu, J., Singh, R., Ma, Y., Zhu, J., Tian, Z., et al. (2012). Electromagnetically induced transparency in terahertz plasmonic metamaterials via dual excitation pathways of the dark mode. *Appl. Phys. Lett.* 100, 131101. doi:10.1063/1.3696306

Liu, P. O., Luxmoore, I. J., Mikhailov, S. A., Savostianova, N. A., Valmorra, F., Faist, J., et al. (2015). Highly tunable hybrid metamaterials employing split-ring resonators strongly coupled to graphene surface plasmons. *Nat. Commun.* 6, 8969. doi:10.1038/ncomms9969

Liu, M., Yang, Q., Xu, Q., Chen, X., Tian, Z., Gu, J., et al. (2018). Tailoring mode interference in plasmon-induced transparency metamaterials. *J. Phys. D. Appl. Phys.* 51, 174005. doi:10.1088/1361-6463/aab6fb

Liu, T., Wang, H., Liu, Y., Xiao, L., Zhou, C., Xu, C., et al. (2018). Independently tunable dual-spectral electromagnetically induced transparency in a terahertz metal–graphene metamaterial. *J. Phys. D. Appl. Phys.* 51, 415105. doi:10.1088/1361-6463/aadb7f

Liu, J., Jin, K., He, X., Zhang, W., Lin, X., Jin, Z., et al. (2019). Independently tunable dual-band plasmon induced transparency enabled by graphene-based terahertz metamaterial. *Appl. Phys. Express* 12, 075010. doi:10.7567/1882-0786/ab27f9

Liu, C., Liu, P., Yang, C., Lin, Y., and Liu, H. (2019). Analogue of dual-controlled electromagnetically induced transparency based on a graphene metamaterial. *Carbon* 142, 354–362. doi:10.1016/j.carbon.2018.10.061

Liu, Z., Zhang, X., Zhou, F., Luo, X., Zhang, Z., Qin, Y., et al. (2021). Triple plasmon-induced transparency and optical switch desensitized to polarized light based on a mono-layer metamaterial. *Opt. Express* 29, 13949–13959. doi:10.1364/OE.425315

Mei, J., Song, C., and Shu, C. (2021). Active manipulation of dual transparency windows in dark-bright-dark mode coupling graphene metamaterial. *Opt. Commun.* 488, 126851. doi:10.1016/j.optcom.2021.126851

Meng, K., Park, S. J., Li, L. H., Bacon, D. R., Chen, L., Chae, K., et al. (2019). Tunable broadband terahertz polarizer using graphene-metal hybrid metasurface. *Opt. Express* 27, 33768–33778. doi:10.1364/OE.27.033768

Novoselov, K. S., Fal′ko, V. I., Colombo, L., Gellert, P. R., Schwab, M. G., and Kim, K. (2012). A roadmap for graphene. *Nature* 490, 192–200. doi:10.1038/nature11458

Shu, C., and Mei, J. (2022). Active and selective manipulation of dual transparency windows in hybrid graphene-vanadium dioxide metamaterial. *Optik* 252, 168519. doi:10.1016/j.ijleo.2021.168519

Su, X., Ouyang, C., Xu, N., Tan, S., Gu, J., Tian, Z., et al. (2015). Dynamic mode coupling in terahertz metamaterials. *Sci. Rep.* 5, 10823. doi:10.1038/srep10823

Sun, D., Qi, L., and Liu, Z. (2020). Terahertz broadband filter and electromagnetically induced transparency structure with complementary metasurface. *Results Phys.* 16, 102887. doi:10.1016/j.rinp.2019.102887

Sun, S., He, Q., Hao, J., Xiao, S., and Zhou, L. (2019). Electromagnetic metasurfaces: Physics and applications. *Adv. Opt. Phot.* 11, 380–479. doi:10.1364/AOP.11.000380

Vakil, A., and Engheta, N. (2011). Transformation optics using graphene. *Science* 332, 1291–1294. doi:10.1126/science.1202691

Venkatesh, S., Lu, X., Saeidi, H., and Sengupta, K. (2020). A high-speed programmable and scalable terahertz holographic metasurface based on tiled CMOS chips. *Nat. Electron.* 3, 785–793. doi:10.1038/s41928-020-00497-2

Wang, J., Fan, J., Shu, H., Liu, C., and Cheng, Y. (2021). Efficiency-tunable terahertz focusing lens based on graphene metasurface. *Opto-Electron. Eng.* 48 (4), 200319. doi:10.12086/oee.2021.200319

Wang, L., Gao, Z., Hou, Z., Song, J., Liu, X., Zhang, Y., et al. (2021). Active modulation of an all-dielectric metasurface analogue of electromagnetically induced transparency in terahertz. *ACS Omega* 6, 4480–4484. doi:10.1021/acsomega.0c06082

Wang, Q., Zhang, X., Xu, Y., Tian, Z., Gu, J., Yue, W., et al. (2015). A broadband metasurface-based terahertz flat-lens array. *Adv. Opt. Mat.* 3, 779–785. doi:10.1002/adom.201400557

Wang, R., Ren, X., Yan, Z., Jiang, L., Sha, W. E. I., and Shan, G. (2019). Graphene based functional devices: A short review. *Front. Phys.* 14 (1), 13603. doi:10.1007/s11467-018-0859-y

Weis, P., Garcia-Pomar, J. L., Höh, M., Reinhard, B., Brodyanski, A., and Rahm, M. (2012). Spectrally wide-band terahertz wave modulator based on optically tuned graphene. *ACS Nano* 6, 9118–9124. doi:10.1021/nn303392s

Wu, T., Shao, Y., Buyingaridi., Ma, S., and Gao, Y. (2021). Terahertz hybrid metal-graphene metamaterials with tunable dual-band electromagnetically induced transparency. *Optik* 240, 166784. doi:10.1016/j.ijleo.2021.166784

Wu, T., Wang, G., Jia, Y., Shao, Y., Chen, C., Han, J., et al. (2021). Dual-spectral plasmon-induced transparent terahertz metamaterial with independently tunable amplitude and frequency. *Nanomaterials* 11, 2876. doi:10.3390/nano11112876

Xiao, S., Wang, T., Liu, T., Yan, X., Li, Z., and Xu, C. (2018). Active modulation of electromagnetically induced transparency analogue in terahertz hybrid metal-graphene metamaterials. *Carbon* 126, 271–278. doi:10.1016/j.carbon.2017.10.035

Xiao, S., Wang, T., Liu, T., Zhou, C., Jiang, X., and Zhang, J. (2020). Active metamaterials and metadevices: A review. *J. Phys. D. Appl. Phys.* 53, 503002. doi:10.1088/1361-6463/abaced

Zhang, S., Genov, D. A., Wang, Y., Liu, M., and Zhang, X. (2008). Plasmon-induced transparency in metamaterials. *Phys. Rev. Lett.* 101, 047401. doi:10.1103/PhysRevLett.101.047401

Zhang, Q., Ma, Q., Yan, S., Wu, F., He, X., and Jiang, J. (2015). Tunable terahertz absorption in graphene-based metamaterial. *Opt. Commun.* 353, 70–75. doi:10.1016/j.optcom.2015.05.017

Zhang, K., Liu, Y., Wu, H., Xia, F., and Kong, W. (2020). Dynamically selective control of dual-mode electromagnetically induced transparency in terahertz metal-graphene metamaterial. *OSA Contin.* 3, 505–514. doi:10.1364/OSAC.380279

Zhang, J., Li, Z., Shao, L., Xiao, F., Xiao, F., and Zhu, W. (2021). Active modulation of electromagnetically induced transparency analog in graphene-based microwave metamaterial. *Carbon* 183, 850–857. doi:10.1016/j.carbon.2021.07.069

Zhang, J., Shao, L., Li, Z., Zhang, C., and Zhu, W. (2022). Graphene-based optically transparent metasurface capable of dual-polarized modulation for electromagnetic stealth. *ACS Appl. Mat. Interfaces* 14, 31075–31084. doi:10.1021/acsami.2c04414

Zhang, J., Li, Z., Zhang, C., Shao, L., and Zhu, W. (2022). Dynamic manipulation of microwave polarization based on anisotropic graphene meta-device. *npj 2D Mat. Appl.* 6, 47. doi:10.1038/s41699-022-00322-8

Zhu, X., Cheng, Y., Fan, J., Chen, F., Luo, H., and Wu, L. (2022). Switchable efficiency terahertz anomalous refraction and focusing based on graphene metasurface. *Diam. Relat. Mat.* 121, 108743. doi:10.1016/j.diamond.2021.108743

Zhu, X., Cheng, Y., Chen, F., Luo, H., and Ling, W. (2022). Efficiency adjustable terahertz circular polarization anomalous refraction and planar focusing based on a bi- layered complementary Z-shaped graphene metasurface. *J. Opt. Soc. Am. B* 39 (3), 705–712. doi:10.1364/JOSAB.446287

Zhuo, S., Zhou, F., Liu, Y., Liu, Z., Zhang, X., Luo, X., et al. (2022). Terahertz multimode modulator based on tunable triple-plasmon-induced transparency in monolayer graphene metamaterials. *J. Opt. Soc. Am. A* 39, 594–599. doi:10.1364/JOSAA.452393